Perchloric acid ($HClO_4$) Drives Atmospheric New Particle Formation Enhanced by Dimethylamine, Ammonia and Sulfuric Acid: Mechanisms and Implications

Shengming Wang[2, 3, #], Ziheng Li[4, #], Xiangli Shi[1, *], Qingzhu Zhang[2], Wenxing Wang[2]

[1]College of Geography and Environment, Shandong Normal University, Jinan 250014, P. R. China

[2]Environment Research Institute, Shandong University, Qingdao 266237, P. R. China

[3]Laboratory of Atmospheric Environment and Pollution Control, Research Center for Eco-Environmental Sciences, Chinese Academy of Sciences, Beijing 100085, China

[4]Shenzhen Univ, Sch Architecture & Urban Planning, Shenzhen, Peoples R China

Keywords: New particle formation, Perchloric acid, Marine aerosol, Particle formation rate, Cluster concentration, Atmospheric nucleation precursor

[#]These authors contributed equally to this paper and should be considered co-first authors.

[*]Corresponding authors. E-mail: shixl@sdnu.edu.cn

Abstract

Recent studies have revealed observations of atmospheric perchloric acid ($HClO_4$, PA) in the Arctic. There are few studies of PA forming aerosol particles in coastal marine regions. We use quantum chemical calculations and Atmospheric Clusters Dynamic Code (ACDC) to compare the enhancement potential of dimethylamine (DMA), ammonia (NH_3), and sulfuric acid (SA) for PA-based new particle formation (NPF). The results show that DMA and NH_3 can strongly interact with PA through hydrogen bonding and proton transfer. Compared with the nucleation of SA, PA nucleates more easily with DMA. Even if the concentration of NH_3 exceeds that of DMA by 10-100 orders of magnitude, the cluster formation rate of PA-DMA cluster formation is much higher than that of the PA-NH_3 cluster system. Clusters with the same number of PA molecules as DMA molecules play a key role in the growth of PA-DMA clusters. The present results reveal the potential for new particle formation of PA in the Arctic boundary layer.

1 Introduction

At least 50% of the overall concentration of aerosol particles in the atmosphere is believed to be attributed to new particle formation (NPF) (Gordon et al., 2017; Takegawa et al., 2020; Williamson et al., 2019; Zhang et al., 2012; Zhao et al., 2024). Because they reflect and absorb solar radiation, reduce visibility, and have an indirect and direct impact on the climate, these aerosols have a deleterious impact on human health(Zhang, 2010). The production mechanism and subsequent expansion of aerosol particles are poorly understood, making them one of the biggest uncertainties in global climate models (Masson-Delmotte et al., 2021). Theoretical studies, laboratory experiments, and field measurements of air aerosols and nucleation events are available (Lee et al., 2019; Chu et al., 2019; Kalivitis et al., 2019). The nucleation of amines and ammonia in the atmosphere using sulfuric acid (SA) is a crucial process in the contaminated boundary layer (Chen et al., 2012; Erupe et al., 2011; Jen et al., 2014; Loukonen et al., 2010; Zhao et al., 2010; Zollner et al., 2012). Nevertheless, SA concentrations in the atmosphere are typically too low to support cluster growth to CCN size. The particle production and subsequent growth stages are significantly influenced by other nucleating agent candidates in the atmosphere.

Abundant atmospheric bases, such as ammonia (NH_3) and alkylamines (methylamine (MA), dimethylamine (DMA), trimethylamine (TMA), and ethylenediamine (EDA) are recognized as important stabilizers for H_2SO_4-driven

nucleation(Almeida et al., 2013; Elm, 2017). A recent theoretical study found that mixed iodic acid-iodous acid (IA-HIO_2) clusters account for the rapid nucleation rate under neutral conditions due to the basicity of iodous acid (HIO_2) and the production of strong halogen bonds(Zhang et al., 2022). By discovering significant perchlorate (ClO_4^-), recent investigations have conjectured the possible formation of perchloric acid ($HClO_4$, PA) in the lower atmosphere (Dasgupta et al., 2005; Rajagopalan et al., 2009; Furdui and Tomassini, 2010; Barrie et al., 1988). Atmospheric PA, the sinking process of chlorine, was initially identified as a significant component in the polar stratosphere (Sander et al., 1989; Webster et al., 1993; Jaeglé et al., 1996). Tham et al. have shown the presence of chlorine oxyacids including chloric acid and PA in the Arctic region, an atmospheric sink for reactive chlorine that has not been previously considered (Tham et al., 2023). The observed concentration ranges of PA is 3×10^4-1×10^6 cm^{-3} in the Arctic atmosphere(Tham et al., 2023). Previous studies have found that chloric acid makes a relatively small contribution to new particle formation(Wang et al., 2025). Engsvang et al. found PA has a high nucleation potential(Engsvang et al., 2024), but the specific nucleation mechanism remain unclear. Perchloric acid is a major component of chlorine oxyacids, and its contribution to new particle formation requires further investigation(Engsvang et al., 2024). The most prevalent and powerful organic base in the environment is dimethylamine (DMA), which significantly accelerates ion-induced and neutral SA-water nucleation (Ge et al., 2011; Jen et al., 2014). During the Arctic summer, alkylamines have been detected at ppt levels(Ferrero et al., 2019). The concentration of dimethylamine (DMA) is estimated

to be between 0.1 and 10 ppt.

In this paper, the nucleation mechanism of $(PA)_{1-4}(DMA)_{1-4}$, $(PA)_{1-4}(NH_3)_{1-4}$, and $(PA)_{1-4}(SA)_{1-4}$ systems are investigated using quantum chemical calculations and the Atmospheric Clusters Dynamic Code (ACDC) methods. Furthermore, the relationships between various components and the thermodynamic characteristics of PA-related clusters were examined. Lastly, ACDC used dynamic simulations to examine the evaporation rates, formation paths, dimer concentrations, and particle formation rates of PA−related clusters using thermodynamic data from three PA−DMA, PA−NH_3, and PA−SA systems.

2 Computational methods

To find the global minimum of the $(PA)_{1-4}(DMA)_{1-4}$, $(PA)_{1-4}(NH_3)_{1-4}$ and $(PA)_{1-4}(SA)_{1-4}$ clusters, we used a multi-step global minimum sampling approach. The ABCluster software was employed to randomly construct the initial structures of 1000 – 10,000 $(PA)_{1-4}(DMA)_{1-4}$, $(PA)_{1-4}(NH_3)_{1-4}$ and $(PA)_{1-4}(SA)_{1-4}$ clusters(Zhang and Dolg, 2015). In addition, the Universal force field (UFF) (Rappé et al., 1992) was used to describe every molecule in the ABCluster software (Zhang and Dolg, 2015). Initially, from structures (>20,00) produced by the artificial bee colony algorithm (Karaboga, 2005) for cluster (ABCluster), 1000 structures with comparatively low energy were selected. In the multistep sampling scheme, the geometry optimization is carried out at the PM7, ωB97X-D/6-31+G(d,p) and ωB97X-D/6-31++G(d,p) levels of

theory, and the single-point energy calculations are executed at the DLPNO-CCSD(T)/aug-cc-pVTZ level of theory based on the ωB97X-D/6-31++G(d,p) theory level. The PM7 and ωB97X-D computations were carried out utilizing the GAUSSIAN 09 program package(Frisch, 2009). ORCA 4.0.0 was implemented to perform DLPNO-CCSD(T) computations(Neese, 2012). The applied computational workflow follows the funnelling approaches originally proposed by Temelso et al. (Temelso et al., 2018) and Kubecka et al.(Kubecka et al., 2019). A large effort has been carried out to identify that the ωB97X-D functional is the best choice for modelling atmospheric molecular clusters. This choice has been based on extensive benchmarks carried out for both the binding energies (Jensen and Elm, 2024; Elm et al., 2013; Elm and Kristensen, 2017) and geometries of atmospheric molecular clusters(Jensen et al., 2022; Knattrup et al., 2026). The fact that the very small and quite old pople style basis set 6-31++G(d,p) is sufficient for modelling atmospheric molecular clusters is also based on extensive benchmarks(Elm and Mikkelsen, 2014; Myllys et al., 2016a; Knattrup et al., 2026). The application of DLPNO in molecular cluster studies was first advocated by Myllys et al (Myllys et al., 2016b)and subsequently benchmarked by Schmitz et al (Schmitz and Elm, 2020). In our DLPNO-CCSD(T) calculations, we employed the NormalPNO convergence criteria as implemented in the ORCA program package. Regarding the treatment of the (T) correction, we used the default non-iterative approach, i.e., DLPNO-CCSD(T0), in which the (T) contribution is evaluated non-iteratively and added to the CCSD energy. Many previous studies have adopted these methods and applied them to a wide range

of acid-base cluster systems(Ning et al., 2026; Zhang et al., 2021; Liu et al., 2023). The initial structures will be modified and re-optimized until the optimization is successful in order to address convergence issues and failures, such as terminating with a false frequency in the optimization of the $(PA)_{1-4}(DMA)_{1-4}$, $(PA)_{1-4}(NH_3)_{1-4}$ and $(PA)_{1-4}(SA)_{1-4}$ cluster geometries. In addition, these computational methods were also applied to CA-PA cluster systems (Figs. S13-S18). PA-DMA clusters' free energy of formation (ΔG) is computed at various temperatures (238, 258, and 278 K). Previous study (Liu et al., 2023) show detailed atmospheric conditions are 253 K at April-2015 in Greenland, 268 K at May-2013 in Ny-Ålesund and 290 K at Aug-2019 in Helsinki. The temperatures of 238 K, 258 K, and 278 K encompass both mid-latitude coastal regions (e.g., Mace Head) and high-latitude regions (e.g., Greenland). The structures of $(SA)_{1–4}$, $(NH_3)_{1–4}$ and $(DMA)_{1–4}$ clusters were obtained from previous studies and are recalculated here(Xie et al., 2017; Ge et al., 2011; Jen et al., 2014; Almeida et al., 2013).

Atmospheric Cluster Dynamics Code (ACDC) Simulation

ACDC was applied to compute the growth pathway, steady-state concentrations, and time-evolving cluster formation rates for the $(PA)_{1–4}(DMA)_{1–4}$, $(PA)_{1–4}(NH_3)_{1–4}$ and $(PA)_{1–4}(SA)_{1–4}$ clusters(Mcgrath et al., 2012). The results of the experiments employing the birth and death equations and the conclusions of the ACDC simulations correspond well(Mcgrath et al., 2012). In this study, ACDC simulations were performed to model the formation process of PA−DMA, PA−NH_3 and PA−SA

neutral clusters without considering the effects of charge and water(Mcgrath et al., 2012). For the studied PA-DMA clusters, the $\beta_{DMA}C_{DMA}/\Sigma\gamma$ of $(PA)_5(DMA)_5$ cluster is greater than 1. The resulting PA-DMA systems $(PA)_5(DMA)_5$ and $(PA)_5(DMA)_4$ clusters are set as boundary clusters. The concentration ranges of [PA], [SA], [DMA] and [NH_3] were defined at 10^6-10^8 cm^{-3}, 10^6-10^8 cm^{-3}, 0.1−100 ppt and 1−100 ppt, respectively(Xie et al., 2017; Ge et al., 2011; Jen et al., 2014; Almeida et al., 2013).

3 Results and discussion

3.1 Cluster structures and cluster formation free energy

Figure 1 displays the $(PA)_{1-4}(DMA)_{1-4}$ clusters identified minimum free energy configurations at the DLPNO-CCSD(T)/aug-cc-pVTZ//ωB97X-D/6-31++G(d,p) level of theory. Proton transfer and hydrogen bonding stabilize the majority of PA−DMA clusters. The formation of halogen bond is not found in PA−DMA clusters. All PA−DMA heteromolecular clusters have been discovered to undergo proton transfer, in which the hydrogen atom of hydroxyl group in the PA molecule moves to the nitrogen atom of the NH_2- group in the DMA to produce N−H...O−Cl hydrogen bond. Each PA molecule donates a proton to a DMA molecule when the quantity of PA molecules and DMA molecules is equal.

When the number of PA molecules is not equal to the number of DMA molecules, the number of proton transfers between PA and DMA depends on the smaller value of the number of PA or DMA molecules. In the PA−NH_3 cluster system (Fig. S1), NH_3

188 accepts hydrogen atoms from the hydroxyl group in PA to generate NH_4^+ and ClO_4^-. It
189 should be noted that when the number of PA molecules is greater than or equal to the
190 number of NH_3 molecules, all NH_3 will be fully protonated. Similar to the PA−DMA
191 cluster system, halogen bonds do not appear in the PA−NH_3 cluster system. The
192 nitrogen atom of NH_3 and the hydrogen atom of the hydroxyl group in PA combine to
193 form the N−H...O−Cl hydrogen bond. However, proton transfer does not take place in
194 any of the PA−SA heteromolecular clusters (Fig. S10). Thus, hydrogen bonds (P−
195 O...H−O and O−H...O−S) and electrostatic interactions sustain the PA−SA cluster
196 system.

197 The Δ*G* values of $(PA)_{1-4}(DMA)_{1-4}$, $(PA)_{1-4}(NH_3)_{1-4}$ and $(PA)_{1-4}(SA)_{1-4}$ clusters
198 at the DLPNO-CCSD(T)/aug-cc-pVTZ//ωB97X-D/6-31++G(d,p) level of 278K, are
199 shown in Figure 2. The Δ*G* values of $(PA)_2$, $(PA)_3$ and $(PA)_4$ clusters are −0.06, −0.99
200 and 2.90 kcal mol^{-1}, respectively, indicating that pure PA molecules are
201 thermodynamically susceptible to forming clusters. The PA−DMA cluster growth is
202 more thermodynamically advantageous than the PA−NH_3 cluster growth, as indicated
203 by the fact that all Δ*G* values of the PA−DMA cluster system are lower than those of
204 the PA−NH_3 cluster system. The $(PA)_{1-4}(DMA)_1$ clusters are 15.15 - 38.79 kcal mol^{-1}
205 lower than those of the corresponding $(PA)_{1-4}$ clusters. The $(PA)_1(DMA)_1$,
206 $(PA)_1(NH_3)_1$, and $(PA)_1(SA)_1$ initial clusters are quite significant in the corresponding
207 cluster systems, with Δ*G* values of −15.15, −9.73, and −4.08 kcal mol^{-1}, respectively.
208 The $(PA)_4(DMA)_4$ cluster has the lowest Δ*G* value, as low as −127.04 kcal mol^{-1}. The
209 PA−SA cluster system exhibits the greatest Δ*G* values among the PA−DMA,

PA−NH_3, and PA−SA cluster systems, suggesting that it is a thermodynamically least stable system. In conclusion, DMA has greater potential for PA-driven nucleation than NH_3 and SA based on the thermodynamic data.

3.2 Evaporation Rates and Cluster Stability

The stability of the PA−DMA, PA−NH_3, and PA−SA cluster systems is further assessed by calculating the evaporation rates at 278 K based on the determined ΔG values. The evaporation rate of DMA-rich clusters is higher than that of PA-rich clusters, as illustrated in Fig. 3, suggesting that clusters with more PA molecules are more stable. $(PA)_1(DMA)_1$, $(PA)_2(DMA)_2$, $(PA)_3(DMA)_3$, and $(PA)_4(DMA)_4$ clusters are all highly stable, with evaporation rates of 8×10^{-2}, 4×10^{-10}, 2×10^{-5}, and 4×10^{-5} s^{-1}, respectively. All pure PA and DMA clusters are unstable, with evaporation rates exceeding 10^9 s^{-1}. The PA−rich hetero molecular clusters are more stable, probably because PA−rich clusters tend to contain more hydrogen bonds and various intermolecular interactions.

With the exception of the $(PA)_4(DMA)_2$, $(PA)_4(DMA)_3$, and $(PA)_4(DMA)_4$ clusters, the evaporation rates of the majority of PA−DMA cluster systems are lower than those of the comparable clusters of PA−NH_3 cluster systems. Similarly, $(PA)_1(NH_3)_1$, $(PA)_2(NH_3)_2$, $(PA)_3(NH_3)_3$, and $(PA)_4(NH_3)_4$ clusters are the stable clusters of the PA−NH_3 cluster system, which have evaporation rates of 3×10^{-2}, 2×10^{-1}, 3×10^{0}, and 2×10^{-8} s^{-1}, respectively. $(PA)_1(SA)_1$ cluster is the most stable cluster with an evaporation rate as high as 6×10^{6} s^{-1} , suggesting the instability of PA−SA clusters.

The actual Gibbs free energies of the PA−DMA systems affected by temperature and vapor concentration were calculated, as shown in Figure. 4. At 278 K, for the PA−DMA cluster system, $(PA)_1(DMA)_1$, $(PA)_2(DMA)_2$, $(PA)_3(DMA)_3$, and $(PA)_4(DMA)_4$ clusters are the primary pathways and the growth process is unimpeded. The fact that the clusters on diagonal has the lowest actual free energy has also been seen in other acid-base systems (Olenius et al., 2013; Elm, 2017). The decreasing trend of the actual Gibbs free energy during the formation of the PA−DMA system is more pronounced with decreasing temperature, implying the thermodynamic stability of the PA−DMA system.

3.3 Steady-State Cluster Concentrations and Nucleation Rate

To further assess the enhancement potential of DMA and NH_3 for PA-driven nucleation, the simulated steady-state PA dimer concentration ($\sum[(PA)_2]$ (cm^{-3})) (a) and the simulated cluster formation rate of the system, J (cm^{-3} s^{-1}) (b), at 278 K as the function of [PA] are shown in Figure. 5. It can be seen that the values of $\sum[(PA)_2]$ and J of the PA-DMA system gradually increase with the increase of [PA] and [DMA] under simulated conditions. However, the effects of [PA] and [DMA] on $\sum[(PA)_2]$ and J values gradually diminish with the increase of [PA] and [DMA]. In the PA-DMA system, neither $\sum[(PA)_2]$ nor J values were saturated with respect to [DMA] at [DMA] = 0.1 - 10 ppt and [PA] = 10^6 - 10^8 cm^{-3}. J values for the SA-DMA cluster system were about 10^{-5} - 10^0 cm^{-3} s^{-1} at 278 K, [DMA] = 1 ppt and [SA] = 10^6- 10^7 cm^{-3} (Xie et al., 2017). J values for the PA-DMA system were about 10^{-1} to 10^3 cm^{-3} s^{-1} at 278

K, [DMA] = 1 ppt and [PA] = 10^6 - 10^7 cm^{-3}. Therefore, the cluster formation rate in the PA-DMA cluster system is 3 to 4 times higher than that in the SA-DMA cluster system. Comparison of the cluster formation rates, J (cm^{-3} s^{-1}), of PA-DMA and PA-NH_3 systems at 278 K; [PA] = 10^6 -10^8 cm^{-3}; [DMA] = 1 ppt; [NH_3] = 100 ppt; CS = 2×10^{-3} s^{-1}, as shown in Fig. 5(c). Even the concentrations of NH_3 are 2 orders of magnitude higher than those of the DMA concentration, the J values of the PA−DMA cluster system are 8-10 orders of magnitude higher than those of the PA−NH_3 cluster system for NH_3 concentrations that are 2 orders of magnitude higher than those of the DMA concentration. This is not an isolated finding(Kurten et al., 2008; Olenius et al., 2013; Elm, 2017; Ortega et al., 2012; Elm et al., 2017; Myllys et al., 2018; Myllys et al., 2019). In addition, the trends of J for the PA-DMA cluster system at temperature of 238, 258 and 298 K; [PA] (10^6 - 10^8 cm^{-3}) and [DMA] (0.1, 1 and 10 ppt) are shown in Fig. 6. As the temperature decreases (from 298 K to 258 K), the J value of the PA-DMA cluster system increases. As also discussed above, this is a direct consequence of lower T leading to a lower free energy and in turn leading to a lower evaporation rate. When the temperature range is 238-258 K, the J value of PA-DMA cluster system tends to be saturated and does not change significantly with temperature. The J value of the PA-DMA system is 1.65 cm^{-3} s^{-1} at 258 K, [DMA]=1 ppt and [PA]=10^6 cm^{-3}.

3.4 Cluster Growth Route

The growth routes of the PA−DMA (a) and PA−NH_3 (b) systems at 278 K, [PA]

= 10^6 cm^{-3}, [DMA] = 3 ppt, and [NH_3] = 100 ppt are shown in Fig. 6. The evaporation rates of $(PA)_2$ and $(DMA)_2$ clusters are 4×10^9 and 2×10^{12} s^{-1}. The higher evaporation rate causes the PA-DMA system to form via the $(PA)_1(DMA)_1$ dimer pathway rather than via the $(PA)_2$ and $(DMA)_2$ cluster pathways. The formation of the $(PA)_1(DMA)_1$ dimer is the initial stage in the PA-DMA system. There is no branching during the growth of clusters of the PA-DMA system, which may be due to the fact that the evaporation rate of clusters on the diagonal (the number of PA molecules is the same as the number of DMA molecules) is much lower than that of clusters off the diagonal (the number of PA molecules is different from the number of DMA molecules). A $(PA)_2(DMA)_2$ cluster complex is then formed by the combination of two $(PA)_1(DMA)_1$ dimer clusters.

$(PA)_2(DMA)_2$ also has only one growth path and further collides with $(PA)_1(DMA)_1$ to form a $(PA)_3(DMA)_3$ cluster. Eventually $(PA)_5(DMA)_5$ clusters is stable enough to grow from the PA-DMA system. Therefore, collision between clusters with PA and DMA monomers is not the main way in the PA-DMA cluster system. Cluster coalescence between a large number of $(PA)_1(DMA)_1$ clusters play an important role in the growth of PA-DMA clusters, which may be due to the low evaporation rate and high stability of $(PA)_1(DMA)_1$, $(PA)_2(DMA)_2$, $(PA)_3(DMA)_3$, and $(PA)_4(DMA)_4$ clusters. This is a usual property of acid-base clusters(Lu et al., 2020). The growth path of the PA-NH_3 cluster system is very similar to that of the PA-DMA cluster system, in which a PA monomer molecule collides with an NH_3 molecule to form a $(PA)_1(NH_3)_1$ dimer cluster, and then $(PA)_1(NH_3)_1$ dimer clusters

298 are continuously added to form $(PA)_4(NH_3)_4$ cluster.

299

300 # 4 Atmospheric Implications and Conclusion

301

302 In this paper, quantum chemical methods are used to study the energy minimum
303 configurations for the formation of atmospheric clusters of PA with DMA, NH_3 and
304 SA in the Arctic boundary layer. The evaporation rates, cluster formation rates and
305 growth paths of the nucleation process of PA with DMA, NH_3 and SA clusters are
306 simulated by inputting ACDC from the thermodynamic data obtained. The following
307 conclusions were drawn:

308 (1) Based on the Gibbs free energies calculated in this study, DMA and NH_3 can
309 strongly interact with PA through hydrogen bonding and proton transfer, thus
310 promoting the formation of PA-DMA and PA-NH_3 clusters. No halogen bonds are
311 found in PA-DMA and PA-NH_3 clusters.

312 (2) Under the condition that the DMA concentration is two orders of magnitude
313 lower than the NH_3 concentration, the formation rate of PA-DMA clusters is much
314 faster than that of PA-NH_3 clusters. The cluster formation rate of the PA-SA cluster
315 system is the slowest among the three systems. This may be due to the fact that no
316 proton transfer occurs between the PA and SA molecules and only hydrogen bonding
317 stabilizes the clusters.

318 (3) The formation rate of pure PA clusters is extremely low. DMA can promote
319 the formation rate of PA clusters to a high level, which reflects the stabilizing effect of

DMA on PA clusters. The results suggest that PA can contribute to new particle formation in the Arctic. The formation of $(PA)_1(DMA)_1$ and $(PA)_1(NH_3)_1$ dimers are the decisive clusters for the growth of PA-DMA and PA-NH_3 cluster systems.

(4) PA can form stable binary clusters with DMA, which is an important step in the formation of new particles in the atmosphere. The nucleation mechanism of PA-DMA revealed in this study may contribute to a deeper understanding of the role of marine chlorine-containing components on marine NPF.

Previous views hold that nucleation involving sulfuric acid/iodine oxoacid and amines/ammonia is a key pathway for new particle formation in the polluted boundary layer. The results of this study provide a partial explanation for the "fate" of PA in the Arctic atmosphere: PA can not only be removed via wet and dry deposition but is also likely to participate in new particle formation by reacting with basic gases (especially DMA) to form stable clusters. This provides a theoretical basis for understanding the role of chlorine-containing components, particularly previously overlooked chlorate, in tropospheric aerosol nucleation. In a region where conventional sulfuric acid-amine/ammonia nucleation is often limited by low precursor concentrations, this PA-DMA pathway offers an additional source of ultrafine particles that can grow into cloud condensation nuclei. This has direct consequences for CCN budgets and, consequently, for cloud microphysical properties and shortwave radiative forcing over the Arctic and other remote marine environments.

This study indicates that perchloric acid has potential in new particle formation

in the Arctic marine boundary layer, particularly in the presence of dimethylamine. This finding has significant atmospheric and climatic implications: first, it reveals a potential new and efficient nucleation pathway between active chlorine released from the ocean (via the formation of $HClO_4$) and nitrogen-containing bases (such as DMA from marine biogenic sources), which may have important implications for assessing the number of cloud condensation nuclei and cloud radiative forcing in the marine boundary layer. Second, it expands our understanding of the atmospheric chlorine cycle, indicating that, in addition to known deposition processes, gas-to-particle transformations involving basic gases represent an important atmospheric "sink" for $HClO_4$. This additional sink may influence the atmospheric residence time and vertical profile of $HClO_4$, with potential ramifications for oxidative capacity and halogen-mediated chemistry in the polar troposphere. These findings underscore the need to revisit how chlorine-containing species are represented in global and regional climate models. Current Earth system models typically neglect $HClO_4$ and its interaction with amines in aerosol nucleation schemes. Incorporating the PA-DMA nucleation mechanism, especially in high-latitude and marine domains, could improve simulations of aerosol-cloud-climate interactions.

Data availability

All data supported the paper are available from the article, supplementary information, and the corresponding author upon reasonable request.

Author Contributions Statement

Shengming Wang: Investigation, Conceptualization, Formal analysis, Data curation, Writing-original draft. **Xiangli Shi:** Methodology, Writing-reviewing and editing, Validation, Supervision. **Qingzhu Zhang:** Methodology, Validation, Supervision, Funding acquisition. **Wenxing Wang:** Resources, Funding acquisition, Writing-reviewing and editing Supervision.

Acknowledgements

The work was financially supported by National Natural Science Foundation of China (project No. 22236004, 21976107, 42075106, 42175122, 4217050207) and Taishan Scholar Foundation of Shandong Province (No. ts201712003).

Additional information

Competing interests: The authors declare no competing financial interests.

References

Almeida, J., Schobesberger, S., Kürten, A., Ortega, I. K., Kupiainen-Määttä, O., Praplan, A. P., Adamov, A., Amorim, A., Bianchi, F., and Breitenlechner, M.: Molecular understanding of sulphuric

acid–amine particle nucleation in the atmosphere, Nature, 502, 359-363, 2013.
Barrie, L., Bottenheim, J., Schnell, R. C., Crutzen, P., and Rasmussen, R.: Ozone destruction and photochemical reactions at polar sunrise in the lower Arctic atmosphere, Nature, 334, 138-141, 1988.
Chen, M., Titcombe, M., Jiang, J., Jen, C., Kuang, C., Fischer, M. L., Eisele, F. L., Siepmann, J. I., Hanson, D. R., and Zhao, J.: Acid – base chemical reaction model for nucleation rates in the polluted atmospheric boundary layer, Proceedings of the National Academy of Sciences, 109, 18713-18718, 2012.
Chu, B., Kerminen, V.-M., Bianchi, F., Yan, C., Petäjä, T., and Kulmala, M.: Atmospheric new particle formation in China, Atmospheric Chemistry and Physics, 19, 115-138, 2019.
Dasgupta, P. K., Martinelango, P. K., Jackson, W. A., Anderson, T. A., Tian, K., Tock, R. W., and Rajagopalan, S.: The origin of naturally occurring perchlorate: the role of atmospheric processes, Environ. Sci. Technol., 39, 1569-1575, 2005.
Elm, J.: Elucidating the limiting steps in sulfuric acid–base new particle formation, The Journal of Physical Chemistry A, 121, 8288-8295, 2017.
Elm, J. and Kristensen, K.: Basis set convergence of the binding energies of strongly hydrogen-bonded atmospheric clusters, Physical Chemistry Chemical Physics, 19, 1122-1133, 2017.
Elm, J. and Mikkelsen, K. V.: Computational approaches for efficiently modelling of small atmospheric clusters, Chemical Physics Letters, 615, 26-29, 2014.
Elm, J., Bilde, M., and Mikkelsen, K. V.: Assessment of binding energies of atmospherically relevant clusters, Physical Chemistry Chemical Physics, 15, 16442-16445, 2013.
Elm, J., Passananti, M., Kurten, T., and Vehkamaki, H.: Diamines can initiate new particle formation in the atmosphere, The Journal of Physical Chemistry A, 121, 6155-6164, 2017.
Engsvang, M., Knattrup, Y., Kubecka, J., and Elm, J.: Chlorine oxyacids potentially contribute to arctic aerosol formation, Environmental Science & Technology Letters, 11, 101-105, 2024.
Erupe, M., Viggiano, A., and Lee, S.-H.: The effect of trimethylamine on atmospheric nucleation involving H 2 SO 4, Atmospheric Chemistry and Physics, 11, 4767-4775, 2011.
Ferrero, L., Sangiorgi, G., Perrone, M. G., Rizzi, C., Cataldi, M., Markuszewski, P., Pakszys, P., Makuch, P., Petelski, T., and Becagli, S.: Chemical composition of aerosol over the Arctic Ocean from summer ARctic EXpedition (AREX) 2011 – 2012 cruises: ions, amines, elemental carbon, organic matter, polycyclic aromatic hydrocarbons, n-alkanes, metals, and rare earth elements, Atmosphere, 10, 54, 2019.
Frisch, A.: gaussian 09W Reference, Wallingford, Usa, 25p, 470, 2009.
Furdui, V. I. and Tomassini, F.: Trends and sources of perchlorate in Arctic snow, Environmental science & technology, 44, 588-592, 2010.
Ge, X., Wexler, A. S., and Clegg, S. L.: Atmospheric amines–Part II. Thermodynamic properties and gas/particle partitioning, Atmos. Environ., 45, 561-577, 2011.
Gordon, H., Kirkby, J., Baltensperger, U., Bianchi, F., Breitenlechner, M., Curtius, J., Dias, A., Dommen, J., Donahue, N. M., and Dunne, E. M.: Causes and importance of new particle formation in the present-day and preindustrial atmospheres, Journal of Geophysical Research: Atmospheres, 122, 8739-8760, 2017.
Jaeglé, L., Yung, Y. L., Toon, G. C., Sen, B., and Blavier, J. F.: Balloon observations of organic and inorganic chlorine in the stratosphere: The role of HClO4 production on sulfate aerosols,

Geophysical research letters, 23, 1749-1752, 1996.
Jen, C. N., McMurry, P. H., and Hanson, D. R.: Stabilization of sulfuric acid dimers by ammonia, methylamine, dimethylamine, and trimethylamine, Journal of Geophysical Research: Atmospheres, 119, 7502-7514, 2014.
Jensen, A. B. and Elm, J.: Massive assessment of the geometries of atmospheric molecular clusters, Journal of Chemical Theory and Computation, 20, 8549-8558, 2024.
Jensen, A. B., Kubecka, J., Schmitz, G., Christiansen, O., and Elm, J.: Massive assessment of the binding energies of atmospheric molecular clusters, Journal of Chemical Theory and Computation, 18, 7373-7383, 2022.
Kalivitis, N., Kerminen, V.-M., Kouvarakis, G., Stavroulas, I., Tzitzikalaki, E., Kalkavouras, P., Daskalakis, N., Myriokefalitakis, S., Bougiatioti, A., and Manninen, H. E.: Formation and growth of atmospheric nanoparticles in the eastern Mediterranean: results from long-term measurements and process simulations, Atmospheric Chemistry and Physics, 19, 2671-2686, 2019.
Karaboga, D.: An idea based on honey bee swarm for numerical optimization, 2005.
Knattrup, Y., Jensen, A. B., and Elm, J.: Coupled Cluster Free Energies for Atmospheric Molecular Clusters: Benchmark and Matching Experimental Free Energies, ACS omega, 11, 36893, 2026.
Kubecka, J., Besel, V., Kurten, T., Myllys, N., and Vehkamaki, H.: Configurational sampling of noncovalent (atmospheric) molecular clusters: sulfuric acid and guanidine, The Journal of Physical Chemistry A, 123, 6022-6033, 2019.
Kurten, T., Loukonen, V., Vehkamäki, H., and Kulmala, M.: Amines are likely to enhance neutral and ion-induced sulfuric acid-water nucleation in the atmosphere more effectively than ammonia, Atmospheric Chemistry and Physics, 8, 4095-4103, 2008.
Lee, S. H., Gordon, H., Yu, H., Lehtipalo, K., Haley, R., Li, Y., and Zhang, R.: New particle formation in the atmosphere: From molecular clusters to global climate, Journal of Geophysical Research: Atmospheres, 124, 7098-7146, 2019.
Liu, L., Li, S., Zu, H., and Zhang, X.: Unexpectedly significant stabilizing mechanism of iodous acid on iodic acid nucleation under different atmospheric conditions, Science of The Total Environment, 859, 159832, 2023.
Loukonen, V., Kurtén, T., Ortega, I., Vehkamäki, H., Padua, A. A., Sellegri, K., and Kulmala, M.: Enhancing effect of dimethylamine in sulfuric acid nucleation in the presence of water – a computational study, Atmospheric Chemistry and Physics, 10, 4961-4974, 2010.
Lu, Y., Liu, L., Ning, A., Yang, G., Liu, Y., Kurtén, T., Vehkamäki, H., Zhang, X., and Wang, L.: Atmospheric sulfuric acid - dimethylamine nucleation enhanced by trifluoroacetic acid, Geophysical Research Letters, 47, e2019GL085627, 2020.
Masson-Delmotte, V., Zhai, P., Pirani, S., Connors, C., Péan, S., Berger, N., Caud, Y., Chen, L., Goldfarb, M., and Scheel Monteiro, P. M.: Ipcc, 2021: Summary for policymakers. in: Climate change 2021: The physical science basis. contribution of working group i to the sixth assessment report of the intergovernmental panel on climate change, 2021.
McGrath, M. J., Olenius, T., Ortega, I., Loukonen, V., Paasonen, P., Kurtén, T., Kulmala, M., and Vehkamäki, H.: Atmospheric Cluster Dynamics Code: a flexible method for solution of the birth-death equations, Atmospheric Chemistry and Physics, 12, 2345-2355, 2012.
Myllys, N., Elm, J., and Kurten, T.: Density functional theory basis set convergence of sulfuric acid-containing molecular clusters, Computational and Theoretical Chemistry, 1098, 1-12, 2016a.
Myllys, N., Elm, J., Halonen, R., Kurten, T., and Vehkamaki, H.: Coupled cluster evaluation of the

stability of atmospheric acid–base clusters with up to 10 molecules, The Journal of Physical Chemistry A, 120, 621-630, 2016b.
Myllys, N., Ponkkonen, T., Passananti, M., Elm, J., Vehkamaki, H., and Olenius, T.: Guanidine: A highly efficient stabilizer in atmospheric new-particle formation, The Journal of Physical Chemistry A, 122, 4717-4729, 2018.
Myllys, N., Kubečka, J., Besel, V., Alfaouri, D., Olenius, T., Smith, J. N., and Passananti, M.: Role of base strength, cluster structure and charge in sulfuric-acid-driven particle formation, Atmospheric Chemistry and Physics, 19, 9753-9768, 2019.
Neese, F.: The ORCA program system, Wiley Interdisciplinary Reviews: Computational Molecular Science, 2, 73-78, 2012.
Ning, A., Mao, L., Zhao, B., Zu, H., Shen, J., Zhao, Y., Li, J., Deng, X., Liu, L., and Zhang, H.: Marine upper-tropospheric rapid particle formation dominated by methanesulfonic acid, Proceedings of the National Academy of Sciences, 123, e2606521123, 2026.
Olenius, T., Kupiainen-Määttä, O., Ortega, I., Kurtén, T., and Vehkamäki, H.: Free energy barrier in the growth of sulfuric acid–ammonia and sulfuric acid–dimethylamine clusters, The Journal of chemical physics, 139, 2013.
Ortega, I. K., Kupiainen, O., Kurtén, T., Olenius, T., Wilkman, O., McGrath, M. J., Loukonen, V., and Vehkamäki, H.: From quantum chemical formation free energies to evaporation rates, Atmospheric Chemistry and Physics, 12, 225-235, 2012.
Rajagopalan, S., Anderson, T., Cox, S., Harvey, G., Cheng, Q., and Jackson, W. A.: Perchlorate in wet deposition across North America, Environ. Sci. Technol., 43, 616-622, 2009.
Rappé, A. K., Casewit, C. J., Colwell, K. S., Goddard III, W. A., and Skiff, W. M.: UFF, a full periodic table force field for molecular mechanics and molecular dynamics simulations, Journal of the American chemical society, 114, 10024-10035, 1992.
Sander, S. P., Friedl, R. R., and Yung, Y. L.: Rate of formation of the ClO dimer in the polar stratosphere: Implications for ozone loss, Science, 245, 1095-1098, 1989.
Schmitz, G. and Elm, J.: Assessment of the DLPNO binding energies of strongly noncovalent bonded atmospheric molecular clusters, ACS omega, 5, 7601, 2020.
Takegawa, N., Seto, T., Moteki, N., Koike, M., Oshima, N., Adachi, K., Kita, K., Takami, A., and Kondo, Y.: Enhanced new particle formation above the marine boundary layer over the Yellow Sea: Potential impacts on cloud condensation nuclei, Journal of Geophysical Research: Atmospheres, 125, e2019JD031448, 2020.
Temelso, B., Morrison, E. F., Speer, D. L., Cao, B. C., Appiah-Padi, N., Kim, G., and Shields, G. C.: Effect of mixing ammonia and alkylamines on sulfate aerosol formation, The Journal of Physical Chemistry A, 122, 1612-1622, 2018.
Tham, Y. J., Sarnela, N., Iyer, S., Li, Q., Angot, H., Quéléver, L. L., Beck, I., Laurila, T., Beck, L. J., and Boyer, M.: Widespread detection of chlorine oxyacids in the Arctic atmosphere, Nature Communications, 14, 1769, 2023.
Wang, S., Zhang, H., Shi, X., Zhang, Q., Wang, W., and Wang, Q.: Chloric acid-driven nucleation enhanced by dimethylamine and sulfuric acid in the Arctic: mechanistic study, Atmospheric Chemistry and Physics, 25, 15359-15368, 2025.
Webster, C., May, R., Toohey, D., Avallone, L., Anderson, J., Newman, P., Lait, L., Schoeberl, M., Elkins, J., and Chan, K.: Chlorine chemistry on polar stratospheric cloud particles in the Arctic winter, Science, 261, 1130-1134, 1993.

Williamson, C. J., Kupc, A., Axisa, D., Bilsback, K. R., Bui, T., Campuzano-Jost, P., Dollner, M., Froyd, K. D., Hodshire, A. L., and Jimenez, J. L.: A large source of cloud condensation nuclei from new particle formation in the tropics, Nature, 574, 399-403, 2019.

Xie, H.-B., Elm, J., Halonen, R., Myllys, N., Kurten, T., Kulmala, M., and Vehkamaki, H.: Atmospheric fate of monoethanolamine: enhancing new particle formation of sulfuric acid as an important removal process, Environmental science & technology, 51, 8422-8431, 2017.

Zhang, J. and Dolg, M.: ABCluster: the artificial bee colony algorithm for cluster global optimization, Physical Chemistry Chemical Physics, 17, 24173-24181, 2015.

Zhang, R.: Getting to the critical nucleus of aerosol formation, Science, 328, 1366-1367, 2010.

Zhang, R., Khalizov, A., Wang, L., Hu, M., and Xu, W.: Nucleation and growth of nanoparticles in the atmosphere, Chemical reviews, 112, 1957-2011, 2012.

Zhang, R., Shen, J., Xie, H.-B., Chen, J., and Elm, J.: The role of organic acids in new particle formation from methanesulfonic acid and methylamine, Atmospheric Chemistry and Physics Discussions, 2021, 1-18, 2021.

Zhang, R., Xie, H.-B., Ma, F., Chen, J., Iyer, S., Simon, M., Heinritzi, M., Shen, J., Tham, Y. J., and Kurten, T.: Critical role of iodous acid in neutral iodine oxoacid nucleation, Environmental Science & Technology, 56, 14166-14177, 2022.

Zhao, B., Donahue, N. M., Zhang, K., Mao, L., Shrivastava, M., Ma, P.-L., Shen, J., Wang, S., Sun, J., and Gordon, H.: Global variability in atmospheric new particle formation mechanisms, Nature, 631, 98-105, 2024.

Zhao, J., Eisele, F. L., Titcombe, M., Kuang, C., and McMurry, P. H.: Chemical ionization mass spectrometric measurements of atmospheric neutral clusters using the cluster-CIMS, Journal of Geophysical Research: Atmospheres, 115, 2010.

Zollner, J., Glasoe, W., Panta, B., Carlson, K., McMurry, P., and Hanson, D.: Sulfuric acid nucleation: power dependencies, variation with relative humidity, and effect of bases, Atmospheric Chemistry and Physics, 12, 4399-4411, 2012.

Figure Captions

Figure 1. Identified minimum free energy configurations of the $(PA)_{1-4}(DMA)_{1-4}$ clusters at the DLPNO-CCSD(T)/aug-cc-pVTZ//ωB97X-D/6-31++G(d,p) level of theory. The atoms of oxygen, nitrogen, chlorine, carbon, and hydrogen are represented by the red, blue, green, gray, and white balls, respectively. Hydrogen bonds are indicated by the dashed white lines.

Figure 2. At the DLPNO-CCSD(T)/aug-cc-pVTZ//ωB97X-D/6-31++G(d,p) level of theory, the formation free energy (ΔG) (in kcal mol^{-1}) of (a) $(PA)_{1-4}(DMA)_{1-4}$, (b) $(PA)_{1-4}(NH_3)_{1-4}$ and (c) $(PA)_{1-4}(SA)_{1-4}$ clusters. The computations are carried out at 1 atm and 278 K.

Figure 3. Evaporation rates for (a) $(PA)_{1-4}(DMA)_{1-4}$ and (b) $(PA)_{1-4}(NH_3)_{1-4}$ (c) $(PA)_{1-4}(SA)_{1-4}$ clusters at 278 K and 1 am.

Figure 4. Actual Gibbs free energy of the PA-DMA clusters at 278, 258 and 238K.

Figure 5. Simulated steady-state PA dimer concentration $\sum[(PA)_2]$ (cm^{-3}) (a) and the cluster formation rates J (cm^{-3} s^{-1}) of the simulation systems (b) as a function of [PA] at 278 K. (c) Comparison of the cluster formation rates J (cm^{-3} s^{-1}) of PA−DMA clusters with PA−NH_3 clusters at 278 K; [PA] = 10^6 −10^8 cm^{-3}; [DMA] = 1 ppt; [NH_3] = 100 ppt; and CS = 2×10^{-3} s^{-1}. The ΔG values at the DLPNO-CCSD(T)/aug-cc-pVTZ//ωB97X-D/6-31++G(d,p) level are used to compute the PA–DMA and PA–NH_3 rates.

Figure 6. The simulated cluster formation rate J (cm^{-3} s^{-1}) of the PA-DMA system at different temperatures (A) 238, (B) 258 K, and (C) 298 K; [PA] = 10^6 −10^8 cm^{-3}; [DMA] = 0.1, 1, and 10 ppt; and CS = 2×10^{-3} s^{-1}.

Figure 7. (a) Main clustering routes of $(PA)_{1-4}(DMA)_{1-4}$ clusters at 278 K, [PA] = 10^6 cm^{-3}, and [DMA] = 3 ppt. (b) Main clustering routes of $(PA)_{1-4}(NH_3)_{1-4}$ clusters at 278 K, [PA] = 10^6 cm^{-3}, and $[NH_3]$ = 100 ppt.

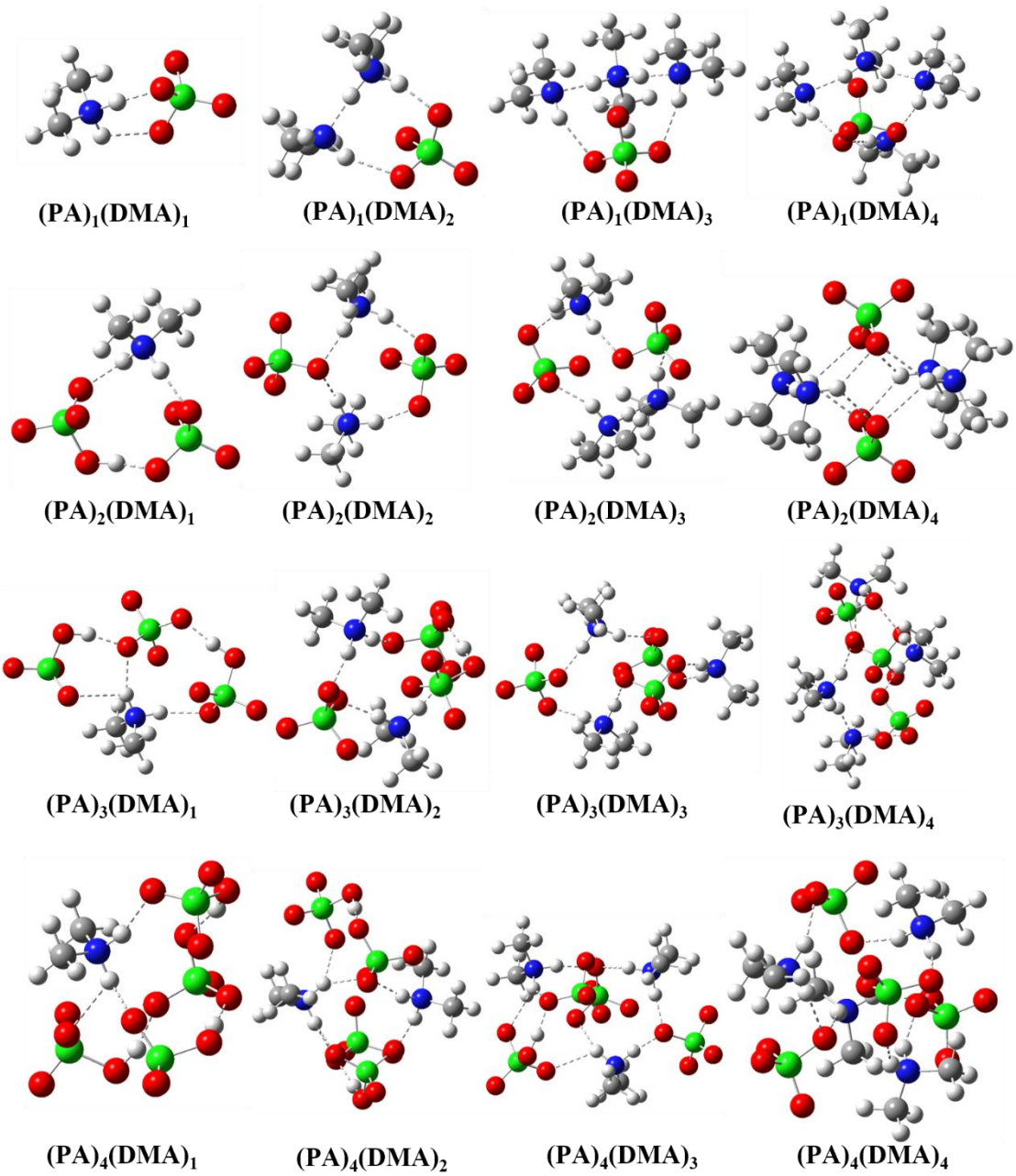

Figure 1. Identified minimum free energy configurations of the $(PA)_{1-4}(DMA)_{1-4}$ clusters at the DLPNO-CCSD(T)/aug-cc-pVTZ//ωB97X-D/6-31++G(d,p) level of

584 theory. The atoms of oxygen, nitrogen, chlorine, carbon, and hydrogen are
585 represented by the red, blue, green, gray, and white balls, respectively. Hydrogen
586 bonds are indicated by the dashed white lines.
587
588

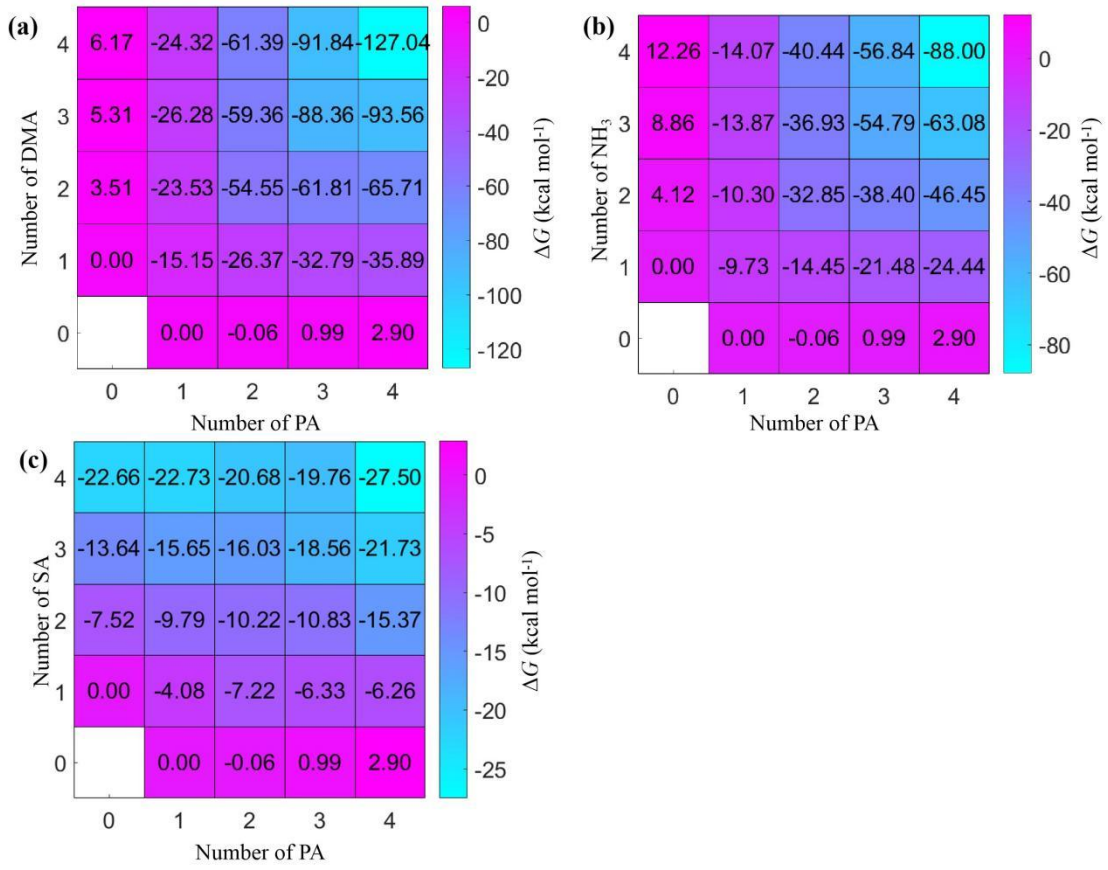

589

590 **Figure 2.** At the DLPNO-CCSD(T)/aug-cc-pVTZ//ωB97X-D/6-31++G(d,p) level of
591 theory, the formation free energy (ΔG) (in kcal mol^{-1}) of (a) $(PA)_{1-4}(DMA)_{1-4}$, (b)
592 $(PA)_{1-4}(NH_3)_{1-4}$ and (c) $(PA)_{1-4}(SA)_{1-4}$ clusters. The computations are carried out at 1
593 atm and 278 K.
594
595

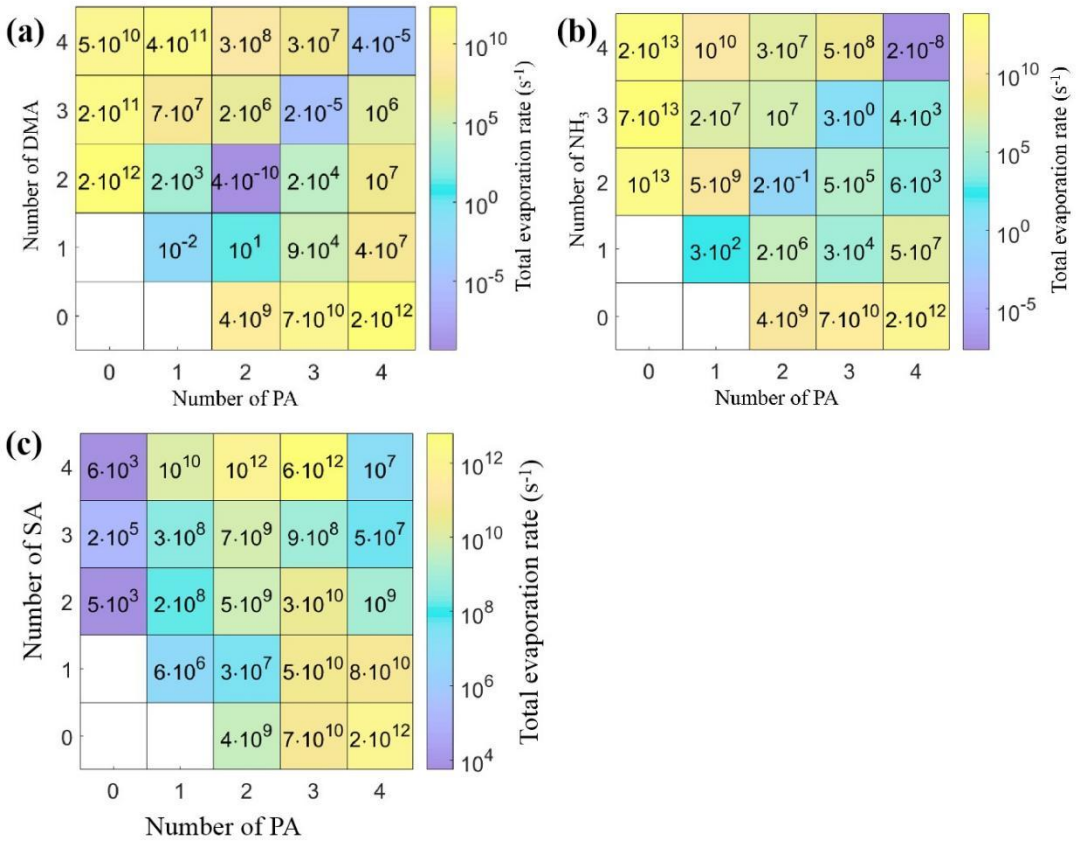

Figure 3. Evaporation rates for (a) $(PA)_{1-4}(DMA)_{1-4}$ and (b) $(PA)_{1-4}(NH_3)_{1-4}$ (c) $(PA)_{1-4}(SA)_{1-4}$ clusters at 278 K and 1 am.

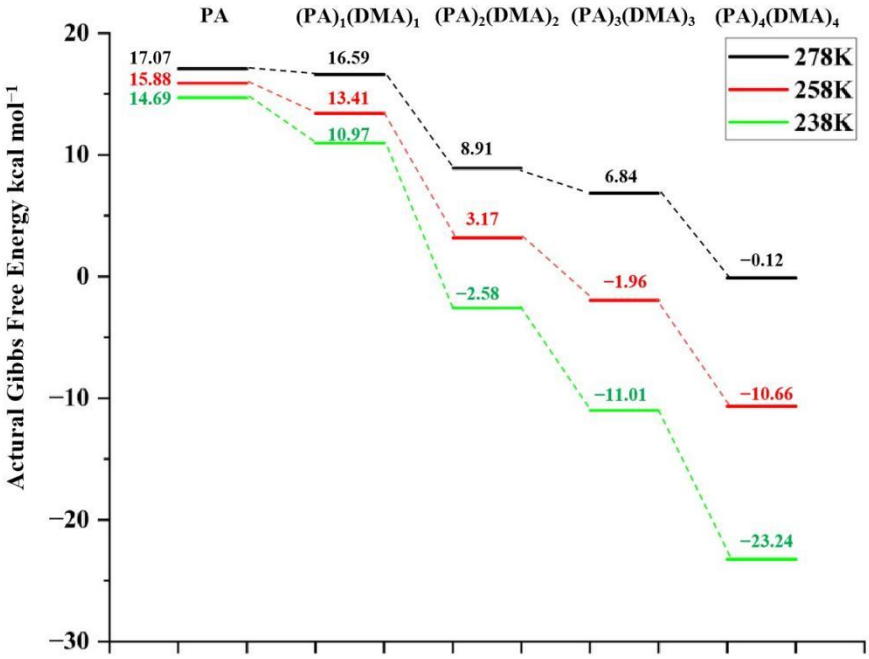

604

605 **Figure 4.** Actual Gibbs free energy of the PA-DMA clusters at 278, 258 and 238K of

606 [PA] = 10^6 cm^{-3}; [DMA] = 3 ppt.

607

608

609

610

611

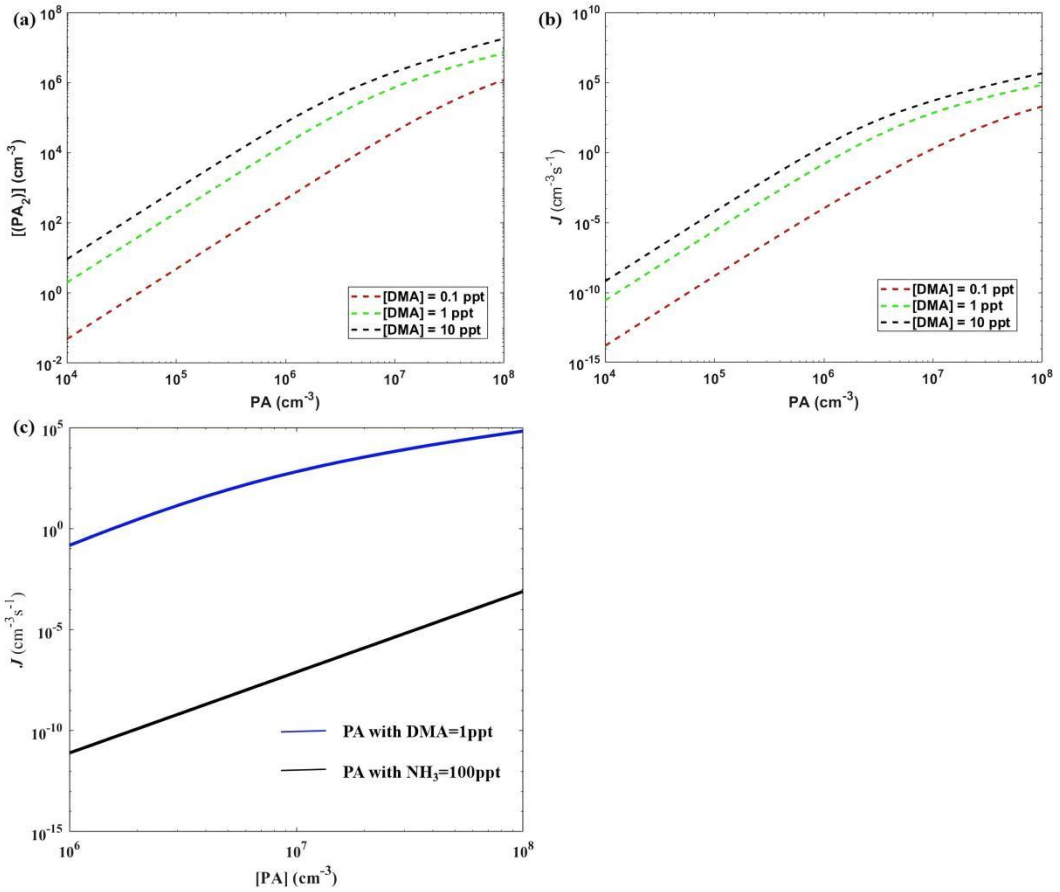

Figure 5. Simulated steady-state PA dimer concentration $\sum[(PA)_2]$ (cm^{-3}) (a) and the cluster formation rates J (cm^{-3} s^{-1}) of the simulation systems (b) as a function of [PA] at 278 K. (c) Comparison of the cluster formation rates J (cm^{-3} s^{-1}) of PA−DMA clusters with PA−NH_3 clusters at 278 K; [PA] = 10^6 −10^8 cm^{-3}; [DMA] = 1 ppt; [NH_3] = 100 ppt; and CS = 2×10^{-3} s^{-1}. The ΔG values at the DLPNO-CCSD(T)/aug-cc-pVTZ//ωB97X-D/6-31++G(d,p) level are used to compute the PA–DMA and PA–NH_3 rates.

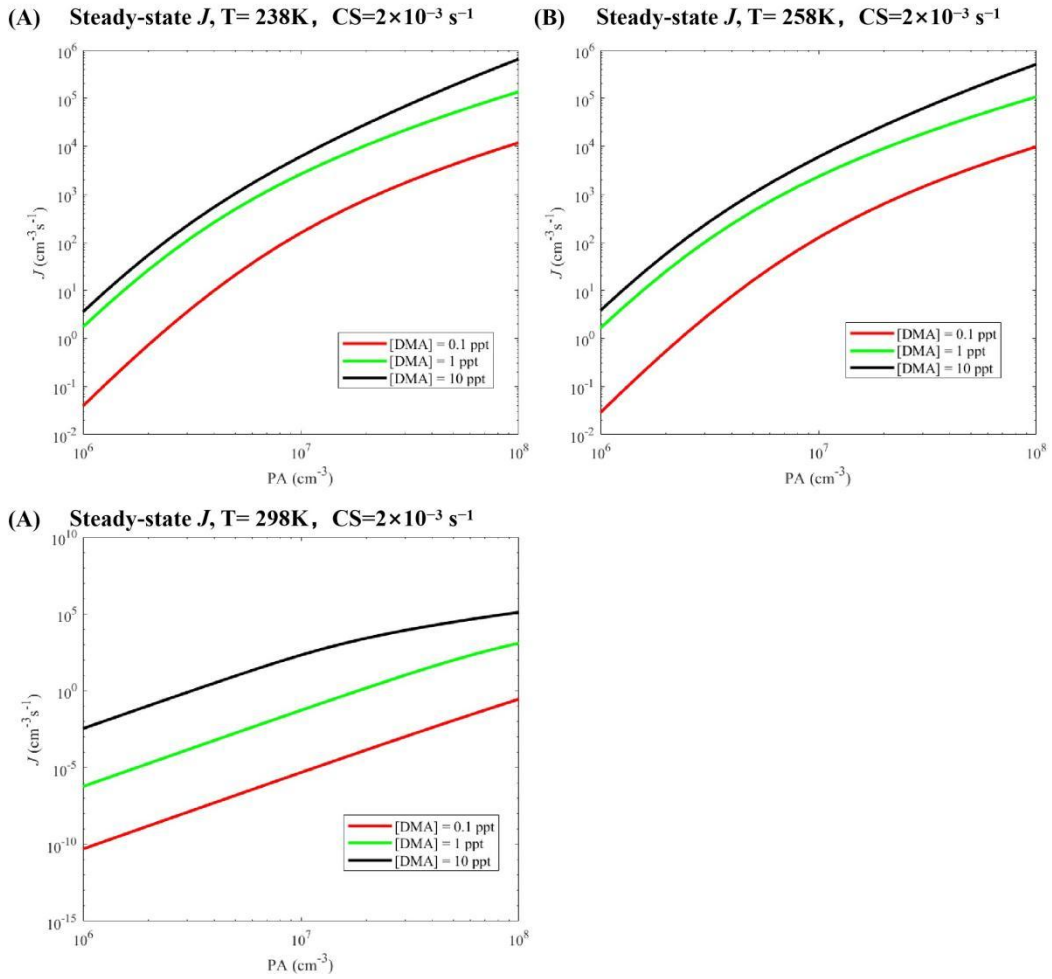

Figure 6. The simulated cluster formation rate J (cm^{-3} s^{-1}) of the PA-DMA system at different temperatures (A) 238, (B) 258 K, and (C) 298 K; [PA] = 10^6 −10^8 cm^{-3}; [DMA] = 0.1, 1, and 10 ppt; and CS = 2×10^{-3} s^{-1}.

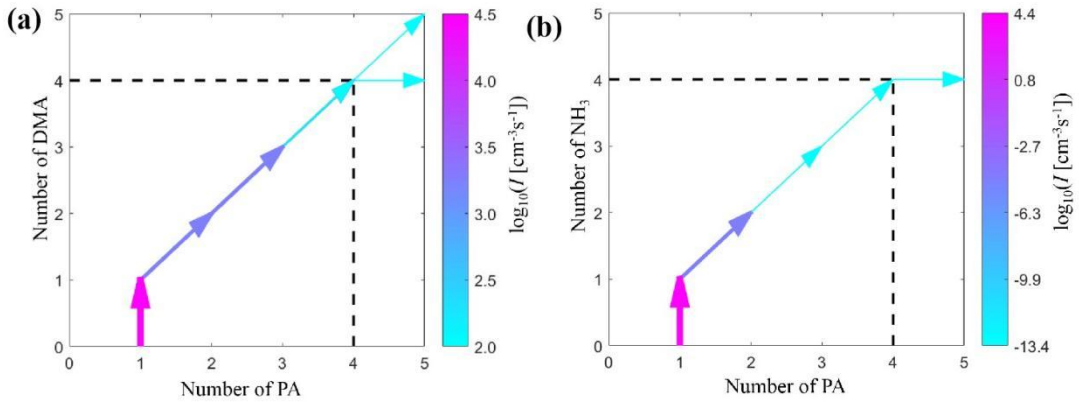

Figure 7. (a) Main clustering routes of $(PA)_{1-4}(DMA)_{1-4}$ clusters at 278 K, [PA] = 10^6 cm^{-3}, and [DMA] = 3 ppt. (b) Main clustering routes of $(PA)_{1-4}(NH_3)_{1-4}$ clusters at 278 K, [PA] = 10^6 cm^{-3}, and [NH_3] = 100 ppt.